ARTICLE

Ti$_3$C$_2$T$_x$ MXene-Based Micro-Supercapacitors with Ultrahigh Volumetric Energy Density for All-in-One Si-Electronics

Haichao Huang, Xiang Chu, Yanting Xie, Binbin Zhang, Zixing Wang, Zhongyi Duan, Ningjun Chen, Zhong Xu, Haitao Zhang, and Weiqing Yang*
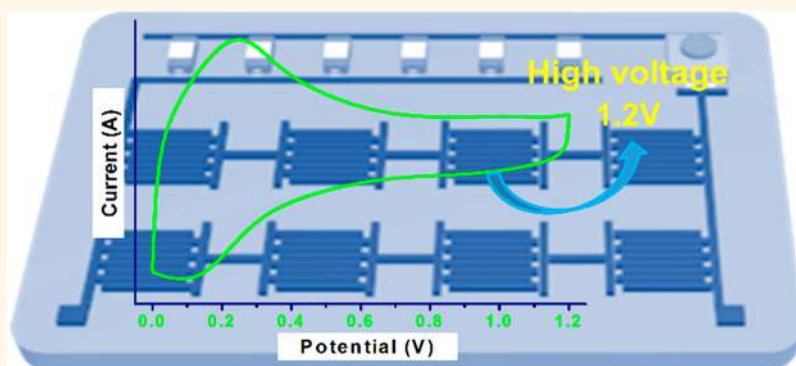
ACCESS | Metrics & More | Article Recommendations | Supporting Information

ABSTRACT: MXene-based microsupercapacitors (MSCs) have promoted the development of on-chip energy storage for miniaturized and portable electronics due to the small size, high power density and integration density. However, restricted energy density and operating voltage invariably create obstacles to the practical application of MSCs. Here, we report a symmetric MXene-based on-chip MSC, achieving an ultrahigh energy density of 75 mWh cm^{-3} with high operating voltage of 1.2 V, which are almost the highest values among all reported symmetric MXene MSCs. The adjustment strategy of acetone on the viscosity and surface tension of MXene ink, along with the natural sedimentation strategy, can effectively prevent the orderly stacking of MXene sheets. Further, we developed an all-in-one Si-electronics with three series MSCs through laser-etching technology, obviously presenting high integration capacity and processing compatibility. Thus, this work will contribute to the development of high integration all-in-one electronics with high energy density MXene-based MSCs.

KEYWORDS: Ti$_3$C$_2$T$_x$ MXene, microsupercapacitors, high operating voltage, high energy density, all-in-one Si-electronics

With the development of microelectronic devices toward miniaturization and high integration, it is urgent to develop corresponding integrated on-chip energy storage devices, especially silicon-compatible devices, to provide required power for these microelectronic units and microsensors.[1−5] Compared with micro battery, on-chip microsupercapacitors (MSCs) with interdigital architecture have become the most viable potential candidate due to their short-term energy storage, burst-mode power delivery, and sustained cycling stability.[6−9] However, restricted energy density always hinders the practical application of MSCs. In general, the energy density is calculated by the equation: $E = 1/2\ CV^2$. Compared with increasing capacity, expanding operating voltage is a more effective way. Therefore, it is a feasible solution to find one material which possesses both

outstanding electrochemical performance and high operating voltage.

As a typical 2D transition metal carbide (MXene), Ti$_3$C$_2$T$_x$ possesses metallic conductivity, abundant chemical properties, and hydrophilic surface, and has been rapidly recognized as a promising electrode material for MSCs.[10−13] Among the previous reports, the achieved Ti$_3$C$_2$T$_x$ MSCs with aqueous
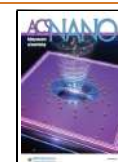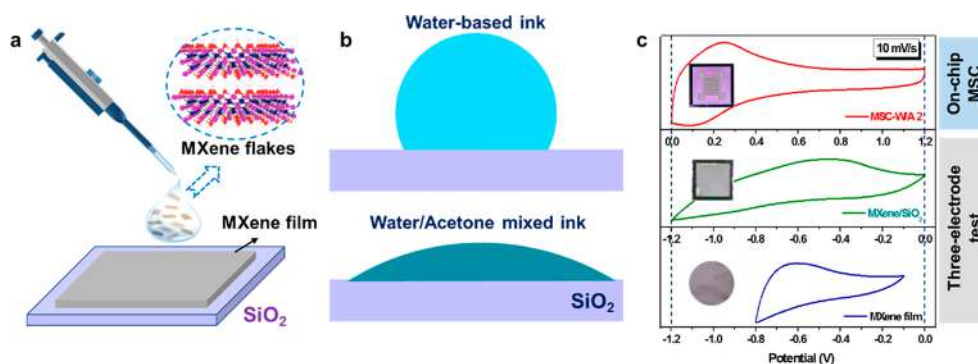
Figure 1. (a) The schematic diagram of the preparation of the MXene-SiO$_2$ electrode via a drop-coating and natural sedimentation strategy. (b) Schematic illustration of the interactions between the surface energy components of MXene ink and Si/SiO$_2$ substrate. With the addition of acetone, the surface energy of the MXene ink will decrease, enabling proper wettability with the wafer. (c) CVs of freestanding MXene film, MXene-SiO$_2$ electrode (a three-electrode system in 1 M H$_2$SO$_4$ electrolyte) and on-chip MSC at a scan rate of 10 mV s^{-1}. MXene-SiO$_2$ electrode and the corresponding MSC have a higher voltage window of 1.2 V than MXene film (0.7 V).

electrolyte has shown high volumetric capacitance (~360 F cm^{-3}) and high energy density (~28 mWh cm^{-3}),[14] which are higher than most MSCs based on other electrode materials, such as graphene,[15,16] carbide-derived carbons,[65] transition metal oxides/hydroxides,[17] and sulfides.[18] Nevertheless, limited by the intrinsic properties of Ti$_3$C$_2$T$_x$ MXene, operating voltage of the previous reported MXene MSCs with aqueous electrolyte is only 0.5−0.8 V, which directly affects the energy density and hinders its practical application.[19] During charge/discharge, Ti$_3$C$_2$T$_x$ presents a continuous change in the titanium oxidation state, producing rectangular-shaped CVs. But over a higher voltage of 0.8 V, the excessive polarization of Ti into TiO and TiO$_2$ will lead to phase change of MXene, accompanied by more hydrogen evolution reaction, which hinders the effective operation of MXene electrode. So it is significant to search for a new approach to further broaden the voltage window of MXene MSCs.

In this work, we successfully assembled a breakthrough volumetric energy density and operating voltage symmetric MSC based on Ti$_3$C$_2$T$_x$ MXene within a PVA/H$_2$SO$_4$ gel electrolyte. To realize the tight connection between MXene and silicon wafer, acetone/water mixed solvent was utilized to tune the rheological properties of MXene ink, particularly surface tension and wettability. In addition, a drop-coating and natural sedimentation strategy was employed to reduce the orderly stacking of MXene flakes. The symmetric MSCs within PVA/H$_2$SO$_4$ gel electrolyte were further fabricated via a laser-etching technology. Surprisingly, the as-prepared symmetric MSC exhibited a volumetric energy density of 75 mWh cm^{-3} (at a power density of 1088 mW cm^{-3} with an ultrahigh operating voltage of 1.2 V), which are almost the highest values among all reported symmetric MXene MSCs. Also, the MSCs exhibited a high areal capacitance of 39.6 mF cm^{-2} at 10 mV s^{-1} (volumetric capacitance of 350.4 F cm^{-3}) and a capacitance retention of ~85.5% after 12 000 cycles. To point it out, MXene acts as a bifunctional material, which simultaneously plays the roles of electrochemical active materials and conductive path, effectively avoiding the metal current collector. These MSCs can be easily integrated with other on-chip microelements through direct predesign of the whole circuit. Based on it, we also developed an all-in-one Si-electronics with MXene MSCs, chip-LEDs and inching-switch, demonstrating high integration and compatibility. Unambigu-

ously, such high operating voltage MXene-based MSCs show great potential in highly integrated electronics and portable devices.

RESULTS AND DISCUSSION

Solution processing is the most widely used technology for manufacturing MXene-based MSCs, since MXenes are mainly synthesized in solutions and possess hydrophilic groups.[20,21] However, the reported solubility of MXenes in organic solvents prepared by conventional schemes is generally low, problematic to meet the practical application.[22] To solve the problem of poor dispersion of MXene in organic solution, some research work has been carried out through intercalation or surface functionalization.[23] In addition, MXene aqueous solution usually have the problems of high surface tension and poor wettability. So it is important to match the physical and chemical properties of MXene (such as rheological properties and terminal groups) with the surface chemistry of the target substrate.[24] To achieve this, acetone aqueous solution was used as the solvent to obtain a high concentration MXene ink with good stability and suitable wettability to SiO$_2$. According to the different volume ratios of water and acetone (W/A = 4:0, 3:1, 2:1, 1:1, 1:2), the blended inks were named as Water, W/A 3, W/A 2, W/A 1, and W/A 0.5, respectively. Generally, when alcohols, aldehydes, and ketones are dissolved in water, the surface tension of water should be reduced. After adding acetone, contact-angle mismatch between MXene ink and SiO$_2$ becomes smaller (Supporting Information (SI) Figure S1), indicating the reduced surface tension and better substrate wettability, enabling better matching with the wafer, along with good adhesion (Figure 1b). The result is that the strengthening of hydrogen bonding between acetone and water will gradually weaken the surface tension of the solutions.[25] Further, as shown in the stylus profiler test (SI Figure S2), the acetone helps the coating, and the coating film exhibits good homogeneity with no obvious coffee ring effect. In contrast, the sedimentation without acetone shows poor uniformity, which can be attributed to the different drying rates of water at different locations.

In addition, the W/A 0.5 ink has a mass fraction of 11.2 mg/mL, much higher than pure water ink (8.3 mg/mL) under the same preparation conditions (SI Figure S3), which guarantees more active material loading on SiO$_2$ substrate. The MXene-SiO$_2$ electrode was obtained through a drop-coating and
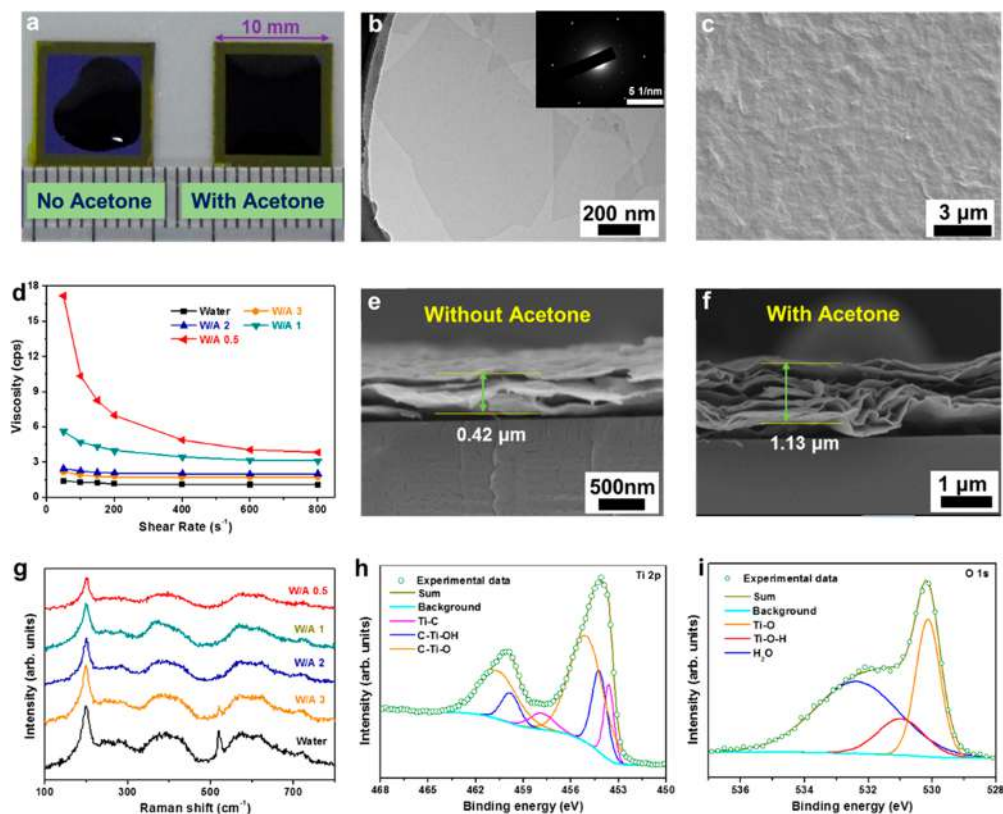
Figure 2. (a) Digital photograph showing the drop-coating process of MXene ink with/without acetone. (b) TEM micrograph and corresponding SAED pattern (inset) of individual $Ti_3C_2T_x$ MXene flakes. (c) SEM image of the surface of MXene-SiO_2 electrode. (d) Viscosity plotted as a function of shear rates for different MXene inks. (e,f) Cross-section SEM images of MXene-SiO_2 electrode. (g) Raman spectra recorded from MXene electrode with different volume ratios of water and acetone (W/A = 4:0, 3:1, 2:1, 1:1, 1:2). (h,i) Deconvoluted high-resolution XPS spectra of Ti 2p and O 1s.

natural sedimentation strategy, as illustrated in Figure 1a. Combined with the strong volatility of acetone and natural sedimentation process, the film displays a much more open structure, which facilitates the access of the ions to interlayers.[26] Besides, other organic solvents, such as ethanol (EA), 1-methyl-2-pyrrolidinone (NMP), ethylene glycol (EG), propylene carbonate (PC), dimethyl sulfoxide (DMSO), and N,N-dimethylformamide (DMF), are also mixed with water in a ratio of 1:1 as a contrast (SI Figure S4). Although MSC-DMSO showed the highest capacitance, it has obvious polarization at 1.2 V (SI Figure S5a). Also, DMSO (NMP, EG, PC) must be dried above 40 degrees Celsius, which may lead to oxidation of MXene flakes Compared with those organic solvents, acetone-mixed ink shows both low surface tension, rapid drying ability, and high capacitance, becoming the optimal choice.

In Figure 1c, the potential window of the as-prepared MXene-SiO_2 electrode has surprisingly reached up to 1.2 V in the three-electrode system (Hg/Hg_2SO_4 electrode as reference electrode), which is considerably higher than freestanding MXene film (0.7 V, Pt acts as a current collector). More importantly, the corresponding on-chip MSCs also exhibit an operating voltage of 1.2 V, higher than almost all reported symmetric MXene MSCs. For this ultrahigh voltage window, we mainly speculate from the following perspectives: (a) the interaction between the unsaturated chemical bond of oxygen on the surface of SiO_2 layer and the MXene flakes leads to exceptional overpotential for hydrogen evolution reaction;[13,25] (b) there may be a built-in electric field at the interface of

MXene-SiO_2 structure, which produces strong electrostatic repulsion to H^+, inhibits hydrogen evolution reaction, and can effectively improve the working voltage of supercapacitor devices.[27] Moreover, MXene MSCs based on other organic solvents mixed ink are obtained in SI Figure S5a. All these MSCs with MXene-SiO_2 electrode exhibit an operating voltage of 1.2 V, while the MXene-Ag electrode has excessive polarized at 1.0 V (SI Figure S5b), demonstrating that the hydrogen bonding between MXene and SiO_2 increases the hydrogen evolution overpotential and expands the voltage window.

Figure 2a demonstrates the digital photograph of MXene inks with/without acetone dripping on the Si/SiO_2 wafer. When acetone is added, the W/A 0.5 ink can quickly cover the entire silicon wafer in a short time of 3 s, and the obtained film is more uniform than without acetone (SI Movie S1). The addition of acetone (low surface tensions of 24.0 mN m^{-1}) into pure water (71.99 mN m^{-1}) will considerably reduce the surface tension and surface energy of the MXene ink, so that the ink can be better dispersed on the silicon wafer with good wettability and adhesion.[25] And from the viscosity-shear rate plots, non-Newtonian characteristics and shear-thinning behavior of ink can be obtained (Figure 2d). As a general trend, the mass fraction and the corresponding viscosity of ink increases as the volume fraction of acetone increases (Figure 2d, SI Figure S2).

Typical transmission electron microscope (TEM) micrographs and corresponding selected area electron diffraction (SAED) patterns of individual $Ti_3C_2T_x$ MXene flakes are shown in Figure 2b and the inset. The $Ti_3C_2T_x$ MXene
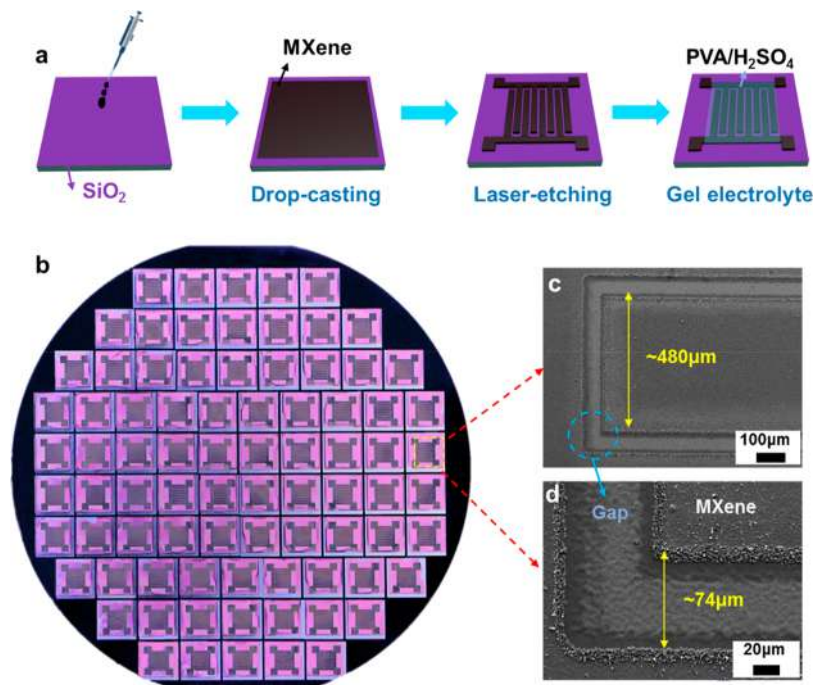
Figure 3. (a) Schematic illustrating the fabrication process of MXene-based on-chip MSC. (b) Digital photograph of the scalable on-chip MSCs. SEM images showing (c) a laser cut MXene finger electrode (width, ~480 μm) and (d) an interspace gap (~74 μm).
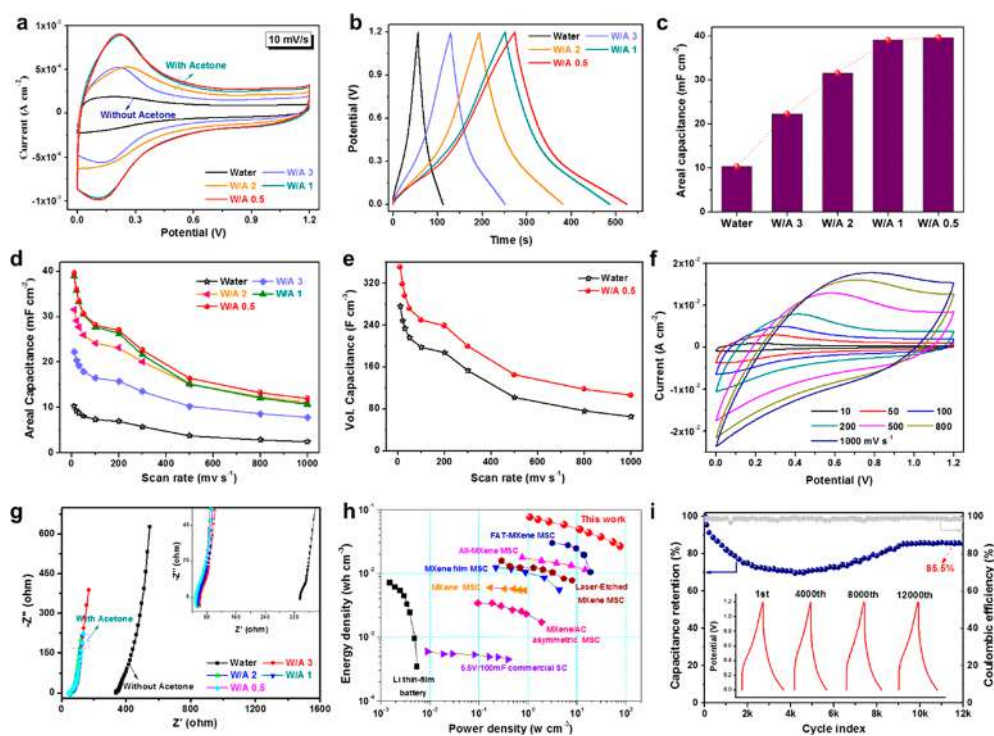

Figure 4. Electrochemical performance of MXene MSCs. (a) CV curves at 10 mV s^{-1} and (b) the corresponding GCD curves at 0.2 mA cm^{-2} of MSCs with different volume ratios of water and acetone (W/A = 4:0, 3:1, 2:1, 1:1, 1:2). (c) Areal capacitance of MSCs with different W/A. (d,e) Areal and volumetric capacitances of on-chip MSCs with different W/A ratios depend on different scan rates. (f) CV curves at the scan rates varying from 10 to 1000 mV s^{-1} for MSC-W/A 0.5. (g) Nyquist plots of these five devices. (h) Ragone plot comparison of this work to other MXene MSC systems. (i) Long-term cycling of on-chip MSCs with current density of 5 mA cm^{-2}. Inset is the typical GCD curves, indicating that the excellent electrochemical performance is not due to parasitic reaction.

nanosheets are flat and nearly transparent. And the corresponding SAED pattern exhibits a typical 6-fold symmetric diffraction pattern with strong diffraction, indicating the high crystallinity of Ti$_3$C$_2$T$_x$ MXene flake.[28] In addition,

the as-obtained Ti$_3$C$_2$T$_x$ MXene film through a drop-coating and natural sedimentation strategy (Figure 2c) is uniform with wrinkles on the surface. The energy dispersive X-ray spectroscopy (EDS) elemental mappings of Ti$_3$C$_2$T$_x$ MXene

film (SI Figure S6) further confirms the elemental composition of electrode materials. The difference in interlayer spacing of MXene nanosheets with/without acetone was also characterized by X-ray diffraction (XRD) (SI Figure S7). The (002) diffraction peak corresponding to an interlayer spacing of MXene nanosheets,[11] shows a minor right shift from 6.3° to 6.5°, indicating a slight decrease of interlayer spacing after addition of acetone. In contrast, from the cross-sectional SEM (Figure 2e,f), the W/A 0.5 film shows a higher thickness of 1.13 μm, displaying a much more open structure, while the MXene film without acetone is only 0.42 μm with a tightly stacked structure. It can be inferred that the high volatility of acetone helps to hinder the restacking phenomenon of 2D Ti$_3$C$_2$T$_x$ MXene flakes during the film fabrication process. The loose structure can enhance the accessibility of ions and realize the effective utilization of MXene flakes.[26] Meanwhile, the presence of acetone can also effectively inhibit the oxidation of MXene flakes, which is conducive to the storage of MXene solution (SI Figure S8).

Raman spectra and X-ray photoelectron spectroscopy (XPS) results were utilized to further understand the structure characteristics and chemical bonds of MXene-SiO$_2$ electrode (Figure 2g−i). The films show typical Raman bands of MXene at 200 and 722 cm^{-1}, assigned to the in-plane A_{1g} vibrational modes of Ti and C atoms.[29] The modes at 283, 390, and 626 cm^{-1} correspond to the E_g group vibrations, including Ti$_3$C$_2$O$_2$, Ti$_3$C$_2$(OH)$_2$, or Ti$_3$C$_2$F$_2$.[29] And the absence of the peak at 144 cm^{-1} suggested that no oxidation was introduced during the film formation process.[30] Further, XPS results were provided to investigate the interfacial features of W/A 0.5 film. The total survey spectrum clearly demonstrated that Ti, C, O, and F were presented on the surface of MXene-SiO$_2$ electrode, as shown in SI Figure S9. Figure 2h shows the high-resolution spectrum of the Ti 2p region, assigned to Ti−C, Ti(II)-O, and Ti(III)-O. In addition, the peak at 458.1 eV can be assigned to TiO$_2$, indicating the oxidation of the MXene flake. In Figure 2i, the three peaks at 530.1, 531.0, and 432.4 eV can be assigned to TiO$_2$, C−Ti−O, and H$_2$O, respectively.[29,31] Therefore, the Raman and XPS results evidently support that the addition of acetone will not affect the surface functional groups of MXene.

Figure 3a illustrates the manufacturing process of MXene-based MSCs on Si/SiO$_2$ wafer. By adjusting the surface tension and wettability of the ink with acetone, MXene can be quickly and evenly dispersed on the Si/SiO$_2$ wafer at room temperature. Then, a drop-coating and natural sedimentation method was employed to obtain the loose-layered MXene film. Moreover, the interdigital pattern was carved through a laser-etching process in a specific center area of 6 × 6 mm^2 (SI Movie S2). PVA/H$_2$SO$_4$ gel electrolyte was carefully dropped onto the surface of the micropattern area. Figure 3b shows a digital photograph of MXene electrodes in a complete silicon chip, indicating the possibility of mass production. The SEM images obviously demonstrate the width and gap of the interdigital pattern are about 480 and 74 μm, respectively (Figure 3c,d). This interdigital structure with a small gap can also facilitate rapid ion migration and increase the effective utilization of the electrode.[32]

The electrochemical performance of MXene-based on-chip MSC was tested by CV, GCD and EIS profiles (Figure 4). The as-fabricated MSCs displays a high operating voltage of 1.2 V, higher than all the reported symmetrical MXene MSCs with aqueous electrolyte (0.5−0.8 V). Since the looser layered structure can provide more substantial accommodations for ion intercalation and deintercalation, MSCs with acetone show higher areal capacitance compared with pure water ink (Figure 4a). The capacity generally increases as the ratio of water to acetone decreases, and remains basically unchanged when the ratio reaches 1:1. From the GCD curves at a current density of 200 μA cm^{-2} (Figure 4b), MSC-W/A 0.5 exhibited the longest discharge time, representing the highest capacitance, which is consistent with CV results. However, calculated from SI Figure S10a, the Coulombic efficiency are 92.3%, 94.2%, 98.4%, 98.8% at the current density of 200, 300, 500, and 1000 μA cm^{-2}, respectively. When the current density decreased to 100 μA cm^{-2}, it is hard to reach 1.2 V (SI Figure S10b). This is because at low current density, part of the charge is used for hydrogen evolution, which caused the low Coulombic efficiency of W/A 0.5. And at higher current density, the W/A 0.5 MSCs show high Coulombic efficiency and good charge−discharge performance (SI Figure S10c). In Figure 4c, the areal capacitance of MSCs with acetone (39.0 mF cm^{-2} at 10 mV s^{-1}) is nearly four times that of pure water (10.3 mF cm^{-2}), due to the higher active substance load and the more open structure brought by rapid evaporation of acetone. Moreover, the two curves of W/A 0.5 and W/A 1 are nearly coincident, indicating that the increase of acetone has little effect on the areal capacitance when the volume ratios of water and acetone reach 1:1 (Figure 4d). In addition, typical CV curves of MSCs-W/A 0.5 at different scan rates were investigated in Figure 4f, which exhibited good rectangular shape up to 1000 mV s^{-1}, representing good capacitance retention. The corresponding volumetric capacitances of these five on-chip MSCs are also calculated from the CVs (Figure 4f, SI Figure S11) and compared in Figure 4e. MSC-W/A 0.5 delivers high volumetric capacitances of 350.1 F cm^{-3}, which is much higher than that of MSCs-Water (276.0 F cm^{-3}). Even at a high scan rate of 1 V s^{-1}, the volumetric capacitances were retained at 106.2 and 65.4 F cm^{-3}.

To further investigate the electrochemical capacitive behavior of these MSCs, the Nyquist plots were obtained in Figure 4g.[13,31,33] The Nyquist plots characterized by a low ion transport resistance and a sharp rise of the imaginary component of impedance at low frequencies, demonstrate the capacitive behavior of the electrode. Compared with MSC-Water, the ohmic resistance of MSC-W/A drops from 337 Ω to around 62 Ω in the high-frequency region. The steeper sloping linear range in the low frequency is related to ion transport resistance in MSC-W/A, demonstrating faster ion diffusion and improved electrochemical kinetics. In this case, more ion channels are available in W/A film due to the looser structure with acetone.

The volumetric energy and power densities of the on-chip MSCs were compared with the reported MXene MSCs, as shown in Figure 4h. Significantly, since the voltage window of on-chip MSCs is broadened to 1.2 V, MSCs-W/A 0.5 delivered an ultrahigh volumetric energy density of 75.5 mWh cm^{-3} at a power density of 1088 mW cm^{-3} and 26.2 mWh cm^{-3} at a high power density of 76.6 W cm^{-3}, which are superior to almost all recently reported MXene-based MSCs, such as FAT-MXene MSC (30 mWh cm^{-3} at 3110 mW cm^{-3}),[14] all-MXene MSC (17.7 mWh cm^{-3} at 758 mW cm^{-3}),[11] MXene film MSC (12.4 mWh cm^{-3} at 221 mW cm^{-3}),[5] MXene/AC asymmetric MSC (3.4 mWh cm^{-3} at 95 mW cm^{-3}),[34] laser-etched MXene MSC (15.8 mWh cm^{-3} at 289 mW cm^{-3}), and MXene/EG MSC (3.6 mWh cm^{-3} at 202 mW cm^{-3}).[28,35] The detailed comparison is summarized in SI Table S1. The outstanding
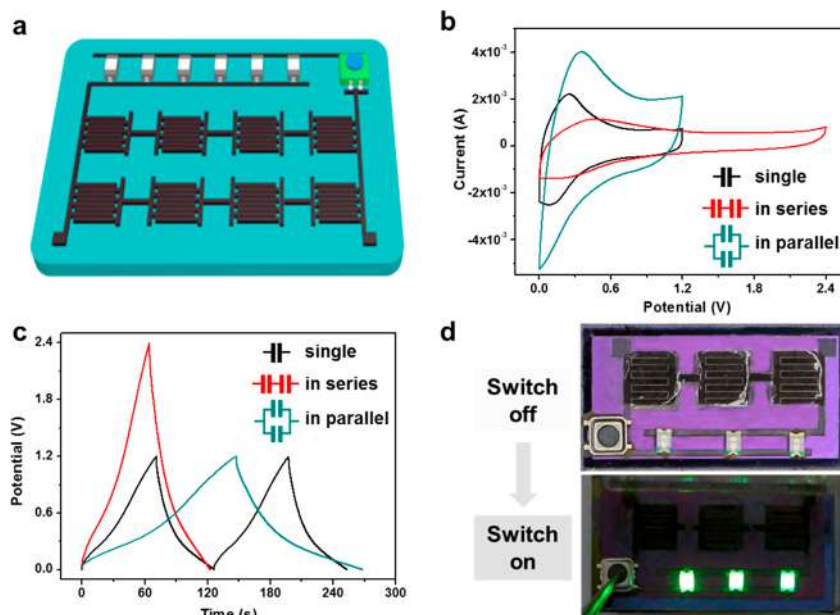
Figure 5. (a) Schematic illustration of the all-in-one Si-electronics via the laser etching technique. (b) CV curves and (c) GCD curves when the MSCs are single, in series, and in parallel connection, respectively. (d) Digital photograph of the all-in-one device with three series MSCs, three chip-LEDs, and one inching-switch. The device can work constantly for around 30 s when switched on.

electrochemical energy output of MSCs-W/A 0.5 lies in the electrochemical characteristics of $Ti_3C_2T_x$, in-plane interdigital electrode, and the loose layer structure. Meanwhile, the devices present good cycling stability, with 85.5% of initial areal capacitance remaining after 12 000 cycles (Figure 4i). The fluctuation of capacitances can be attributed to the hydrogen evolution reaction during charge and discharge. As shown in SI Figure S12, during cycle test, the negative electrode gradually generates bubbles originated from the hydrogen evolution reaction, which prevents ions from reaching the electrode surface and seriously attenuates the capacitance of MSCs. After thousands of cycles, hydrogen evolution reaction gradually disappeared, the capacitance increases, and finally remains stable. Self-discharge behavior is also an important factor to measure the performance of MSCs. As shown in SI Figure S13, the MSCs with acetone show much better self-discharge performance than MSCs without acetone. It is speculated that the considerable nonuniformity of MXene electrode (MSCs-Water) leads to micro contact between electrodes during the laser etching process, resulting in serious self-discharge.

To meet more practical applications with high voltage and energy, on-chip MSCs need to be integrated in series or in parallel. Due to the outstanding wettability and high conductivity, MXene can serve as both electrochemical active materials and current collectors, easily realizing the all-in-one Si-based electronics through a laser-etching process (Figure 5a). The CV curves of single MSC, two in series or in parallel show a similar shape (Figure 5b), indicating the uniformity of each MSC unit. Two MSCs connected in series display a larger voltage window of 2.4 V, while two devices connected in parallel displays twice the capacity of a single MSC (integration area of the CV curve). Besides, at the same current density, discharge time of two MSCs in parallel is about twice that of single MSC, while the two MSCs in series is nearly unchanged (Figure 5c). Importantly, $Ti_3C_2T_x$ MXene with outstanding conductivity could constitute the whole circuit without other metal collectors, which can be easily integrated with other

microelectronics. Figure 5d exhibits the digital photographs of the all-in-one devices with three series MSCs, three chip-LEDs and one inching-switch, before and after the switch is turned on. With three MSCs connected in series, the highly integrated device can output a voltage of 3.6 V and light the chip-LEDs for around 30 s (SI Movie S3).

The extraordinary performance of the MXene-based micro-supercapacitors in PVA/H_2SO_4 gel electrolyte including high operating voltage, high volumetric energy density, and high integration should be ascribed to the following reasons: (i) the high concentration MXene ink with good wettability in acetone aqueous solution can match well with the SiO_2/Si wafer; (ii) volatile acetone and natural sedimentation process hinder the restacking phenomenon of 2D $Ti_3C_2T_x$ MXene flakes and make the film a much more open structure, which can facilitate the access of the ions and realize the effective utilization of MXene flakes; (iii) the hydrogen bonding between MXene and SiO_2 surface increases the hydrogen evolution overpotential and expands the voltage window to 1.2 V, greatly promoting the increase of energy density; (iv) all-MXene architecture ensures integration accessibility and high compatibility. Therefore, this work demonstrates that the proposed on-chip MSCs can achieve large-scale production and integration for practical applications.

CONCLUSION

In summary, we have demonstrated the symmetric on-chip MSCs with MXene blended ink for all-in-one Si-electronics. The as-fabricated MSCs delivered a high volumetric capacitance of 350.4 F cm^{-3} with high operating voltage of 1.2 V, corresponding to the breakthrough volumetric energy density of 75.5 mWh cm^{-3} for MXene-based MSCs. Moreover, the MSCs can be easily integrated with other on-chip electronics, which can effectively increase the integration density. Therefore, the established MSCs based on solution inks of MXene may contribute to the development of high-performance and highly integrated all-in-one Si-electronics.

METHODS

Preparation of Multilayer-Ti$_3$C$_2$T$_x$. The multilayer-Ti$_3$C$_2$T$_x$ (m-Ti$_3$C$_2$T$_x$) was prepared by wet etching of Ti$_3$AlC$_2$ MAX phase. In detail, 2 g of lithium fluoride was added to 40 mL of 9 M HCl and stirred for 10 min. Then, 2 g of Ti$_3$AlC$_2$ (400 mesh, 11 technology Co., Ltd.) was slowly added to the acidic etchant solution and maintained at 40 °C for 24 h under constant stirring. After that, the resultant dark mixture was washed repeatedly with deionized water by centrifugation at 4000 rpm for 5 min until the pH of supernatant exceeded 6. The clay-like sediment (m-Ti$_3$C$_2$T$_x$) at the bottom was collected and vacuum-dried.

Preparation of MXene Ink. The MXene ink was simply prepared by further sonicating m-Ti$_3$C$_2$T$_x$ solution. Briefly, 0.1 g of m-Ti$_3$C$_2$T$_x$ was added to 4 mL of the water/acetone mixed solution, followed by sonication in an ice bath for 60 min. The ratios of water and acetone are 4:0, 3:1, 2:1, 1:1, and 1:2, and the obtained samples were designated as Water, W/A 3, W/A 2, W/A 1, and W/A 0.5, respectively. Then the supernatant (MXene ink) was collected by centrifugation at 3500 rpm for 60 min, and the remaining sediment was vacuum-dried. The mass fraction of MXene ink was calculated by dividing the mass difference before and after centrifugation by the volume of solution, which is about 8.3, 7.2, 7.9, 10.6, and 11.2 mg/mL respectively, corresponding to Water, W/A 3, W/A 2, W/A 1, and W/A 0.5.

Fabrication of All-MXene Symmetric MSCs. The preparation of PVA-H$_2$SO$_4$ gel electrolyte has been described in our previous study. The drop-coating and natural sedimentation method following with a laser-etching process was performed to fabricate the MXene-based interdigital electrode. First, 20 μL of the MXene ink was dropped on the tape-masked Si/SiO$_2$ wafer (8 × 8 mm), followed by natural sedimentation and drying. Then, the MXene film is processed into interdigital electrode by laser-etching, and damage of the silicon dioxide layer by laser should be avoided. After that, PVA/H$_2$SO$_4$ gel electrolyte was dropped onto the interdigital part. After vaporizing the excess water overnight, MXene-based symmetric MSCs were obtained. Finally, an additional PDMS layer covered the gel electrolyte as a passivation layer to enhance stability.

Characterization. The surface morphology and structure were investigated with a scanning electron microscope system (SEM, FEI QUANTA FEG 250, American) and a transmission electron microscope (TEM, JEOL JEM-2100, Japan). And the elemental distribution was obtained by energy dispersive X-ray spectroscopy (EDS, FEI QUANTA FEG 250, American). X-ray diffraction (XRD) patterns of the samples were obtained with a powder diffractometer (PANalytical X'Pert Powder diffractometer, Holland) under Cu Kα radiation. The Raman spectrum was determined using a HORIBA Jobin-Yvon XploRA ONE contocal Raman microscope with 532 nm laser. The X-ray photoelectron spectroscopy (XPS) data was obtained with a Thermo Scientific ESCALAB 250Xi spectrometer. The rheological behavior of the inks was tested at room temperature using a DHR-2 rheometer (TA Instruments) with a 20 mm parallel plate geometry and a 900 μm gap.

Electrochemical Measurements. The electrochemical characterization of MXene film and MXene-SiO$_2$ electrode were conducted using a three-electrode system (with Hg/Hg$_2$SO$_4$ electrode as reference electrode in 1 M H$_2$SO$_4$ electrolyte). Cyclic voltammetry (CV) curves at scan rates of 10−1000 mV s^{-1} in the potential window of 0 to 1.2 V, galvanostatic charge/discharge (GCD) tests at a current density of 0.2−10 mA cm^{-2}, and electrochemical impedance spectroscopy (EIS) recorded in the frequency range of 10 kHz to 0.1 Hz of the MSCs were measured with an electrochemical workstation (CHI660E, Chenhua, China). The areal capacitance (C_A), the volumetric capacitance (C_V), the volumetric energy density (E_V), the volumetric energy density (E_V), and the volumetric power density (P_V) were calculated as follows:

$$C_A = \int_{V1}^{V2} I(V)dV/(2v\Delta V \cdot A)(\mathrm{mFcm^{-2}}) \tag{1}$$

$$C_V = C_A/d(\mathrm{Fcm^{-3}}) \tag{2}$$

$$E_V = C_V \cdot V^2/(2 \cdot 3.6)(\mathrm{mWhcm^{-3}}) \tag{3}$$

$$P_V = 3.6E_V/\Delta t(\mathrm{mWcm^{-3}}) \tag{4}$$

where I is the current, v is the scanning rate, ΔV is the voltage window, V_2 and V_1 are the bounds of the potential window, A is the geometrical area of the effective MSC electrode, d is the thickness of MXene electrode, and t is the total discharge time, respectively.

ASSOCIATED CONTENT

⒮ Supporting Information

The Supporting Information is available free of charge at https://pubs.acs.org/doi/10.1021/acsnano.1c08172.

Contact-angle test between different MXene ink and SiO$_2$; thickness of MXene film from step profiler; mass fraction of MXene ink; digital photograph of MXene ink; CV curves of MSCs based on MXene ink with different organic solvents; EDS images; XRD of Ti$_3$C$_2$T$_x$ MXene film; XRD of MXene with/without acetone after different days; XPS full spectrum; GCD curves of MSC-W/A 0.5; CV curves of MSCs; optical microscope photographs showing the appearance of bubbles; self-discharge performance of MSCs (PDF)

Movie S1: Drop coating process of different MXene ink (MP4)

Movie S2: Laser etching process electrode machining (MP4)

Movie S3: Display of integrated devices (MP4)

AUTHOR INFORMATION

Corresponding Author

Weiqing Yang − *Key Laboratory of Advanced Technologies of Materials, Ministry of Education, School of Materials Science and Engineering, Southwest Jiaotong University, Chengdu 610031, China;* ⓘ orcid.org/0000-0001-8828-9862; Email: wqyang@swjtu.edu.cn

Authors

Haichao Huang − *Key Laboratory of Advanced Technologies of Materials, Ministry of Education, School of Materials Science and Engineering, Southwest Jiaotong University, Chengdu 610031, China*

Xiang Chu − *Key Laboratory of Advanced Technologies of Materials, Ministry of Education, School of Materials Science and Engineering, Southwest Jiaotong University, Chengdu 610031, China*

Yanting Xie − *Key Laboratory of Advanced Technologies of Materials, Ministry of Education, School of Materials Science and Engineering, Southwest Jiaotong University, Chengdu 610031, China*

Binbin Zhang − *Key Laboratory of Advanced Technologies of Materials, Ministry of Education, School of Materials Science and Engineering, Southwest Jiaotong University, Chengdu 610031, China*

Zixing Wang − *Key Laboratory of Advanced Technologies of Materials, Ministry of Education, School of Materials Science and Engineering, Southwest Jiaotong University, Chengdu 610031, China*

Zhongyi Duan − *Key Laboratory of Advanced Technologies of Materials, Ministry of Education, School of Materials Science and Engineering, Southwest Jiaotong University, Chengdu 610031, China*

Ningjun Chen − *Key Laboratory of Advanced Technologies of Materials, Ministry of Education, School of Materials Science and Engineering, Southwest Jiaotong University, Chengdu 610031, China*

Zhong Xu − *Key Laboratory of Advanced Technologies of Materials, Ministry of Education, School of Materials Science and Engineering, Southwest Jiaotong University, Chengdu 610031, China*

Haitao Zhang − *Key Laboratory of Advanced Technologies of Materials, Ministry of Education, School of Materials Science and Engineering, Southwest Jiaotong University, Chengdu 610031, China;* ◉ orcid.org/0000-0002-2057-7654

Notes
The authors declare no competing financial interest.

REFERENCES

(1) El-Kady, M.; Kaner, R. Scalable Fabrication of High-Power Graphene Micro-Supercapacitors for Flexible and On-Chip Energy Storage. *Nat. Commun.* **2013**, *4*, 1475.

(2) Huang, P.; Lethien, C.; Pinaud, S.; Brousse, K.; Laloo, R.; Turq, V.; Respaud, M.; Demortiere, A.; Daffos, B.; Taberna, P. L. On-Chip and Freestanding Elastic Carbon Films for Micro-Supercapacitors. *Science* **2016**, *351*, 691−695.

(3) Guo, R.; Chen, J.; Yang, B.; Liu, L.; Su, L.; Shen, B.; Yan, X. In-Plane Micro-Supercapacitors for an Integrated Device on One Piece of Paper. *Adv. Funct. Mater.* **2017**, *27* (43), 1702394.

(4) Gong, H.; Chen, S.; Ning, R.; Chang, T.; Tok, J.; Bao, Z. Densely Packed and Highly Ordered Carbon Flower Particles for High Volumetric Performance. *Small Sci.* **2021**, *1*, 2000067.

(5) Huang, H.; He, J.; Wang, Z.; Zhang, H.; Jin, L.; Chen, N.; Xie, Y.; Chu, X.; Gu, B.; Deng, W.; Yang, W. Scalable, and Low-cost Treating-Cutting-Coating Manufacture Platform for MXene-Based On-Chip Micro-Supercapacitors. *Nano Energy* **2020**, *69*, 104431.

(6) Chmiola, J.; Largeot, C.; Taberna, P.; Simon, P.; Gogotsi, Y. Monolithic Carbide-Derived Carbon Films for Micro-Supercapacitors. *Science* **2010**, *328* (5977), 480.

(7) Feng, D.; Lv, Y.; Wu, Z.; Dou, Y.; Han, L.; Sun, Z.; Xia, Y.; Zheng, G.; Zhao, D. Free-Standing Mesoporous Carbon Thin Films with Highly Ordered Pore Architectures for Nanodevices. *J. Am. Chem. Soc.* **2011**, *133* (38), 15148.

(8) Chu, X.; Zhao, X.; Zhou, Y.; Wang, Y.; Han, X.; Zhou, Y.; Ma, J.; Wang, Z.; Huang, H.; Xu, Z.; Yan, C.; Zhang, H.; Yang, W.; Chen, J. An ultrathin robust polymer membrane for wearable solid-state electrochemical energy storage. *Nano Energy* **2020**, *76*, 105179.

(9) Cui, Y.; Cao, Z.; Zhang, Y.; Chen, H.; Gu, J.; Du, Z.; Shi, Y.; Li, B.; Yang, S. Single-Atom Sites on MXenes for Energy Conversion and Storage. *Small Sci.* **2021**, *1*, 2100017.

(10) Huang, L.; Ding, L.; Wang, H. MXene-Based Membranes for Separation Applications. *Small Sci.* **2021**, *1*, 2100013.

(11) Peng, Y.; Akuzum, B.; Kurra, N.; Zhao, M.; Alhabeb, M.; Anasori, B.; Kumbur, E.; Alshareef, H.; Ger, M.; Gogotsi, Y. All-MXene (2D Titanium Carbide) Solid-State Microsupercapacitors for On-Chip Energy Storage. *Energy Environ. Sci.* **2016**, *9* (9), 2847−2854.

(12) Huang, H.; Chu, X.; Su, H.; Zhang, H.; Xie, Y.; Deng, W.; Chen, N.; Liu, F.; Zhang, H.; Gu, B.; Deng, W.; Yang, W. Massively Manufactured Paper-Based All-Solid-State Flexible Micro-Supercapacitors with Sprayable MXene Conductive Inks. *J. Power Sources* **2019**, *415*, 1−7.

(13) Lukatskaya, M.; Kota, S.; Lin, Z.; Zhao, M.; Shpigel, N.; Levi, M.; Halim, J.; Taberna, P.; Barsoum, M.; Simon, P.; Gogotsi, Y. Ultra-High-Rate Pseudocapacitive Energy Storage in Two-Dimensional Transition Metal Carbides. *Nat. Energy* **2017**, *2* (8), 17105.

(14) Huang, X.; Wu, P. A Facile, High-yield, and Freeze-and-Thaw-Assisted Approach to Fabricate MXene with Plentiful Wrinkles and Its Application in On-Chip Micro-Supercapacitors. *Adv. Funct. Mater.* **2020**, *30* (12), 1910048.

(15) Wu, Z.; Parvez, K.; Feng, X.; Müllen, K. Photolithographic Fabrication of High-Performance All-Solid-State Graphene-Based Planar Micro-Supercapacitors with Different Interdigital Fingers. *J. Mater. Chem. A* **2014**, *2* (22), 8288.

(16) Komeily-Nia, Z.; Qu, L.; Li, J. Progress in the Understanding and Applications of the Intrinsic Reactivity of Graphene-Based Materials. *Small Sci.* **2021**, *1* (2), 2000026.

(17) Yang, Q.; Li, Z.; Zhang, R.; Zhou, L.; Shao, M.; Wei, M. Carbon Modified Transition Metal Oxides/Hydroxides Nanoarrays toward High-Performance Flexible All-Solid-State Supercapacitors. *Nano Energy* **2017**, *41*, 408−416.

(18) Naderi, L.; Shahrokhian, S. Nickel Vanadium Sulfide Grown on Nickel Copper Phosphide Dendrites/Cu Fibers for Fabrication of All-Solid-State Wire-Type Micro-Supercapacitors. *Chem. Eng. J.* **2020**, *392*, 124880.

(19) Lukatskaya, M.; Bak, S.; Yu, X.; Yang, X.; Barsoum, M.; Gogotsi, Y. Probing the Mechanism of High Capacitance in 2D Titanium Carbide using in Situ X-Ray Absorption Spectroscopy. *Adv. Energy Mater.* **2015**, *5* (15), 1500589.

(20) Zhang, Y.; Wang, Y.; Jiang, Q.; El-Demellawi, J.; Kim, H.; Alshareef, H. MXene Printing and Patterned Coating for Device Applications. *Adv. Mater.* **2020**, *32* (21), 1908486.

(21) Zhang, C.; Kremer, M.; Seral-Ascaso, A.; Park, S.; McEvoy, N.; Anasori, B.; Gogotsi, Y.; Nicolosi, V. Stamping of Flexible, Coplanar Micro-Supercapacitors using MXene Inks. *Adv. Funct. Mater.* **2018**, *28* (9), 1705506.

(22) Maleski, K.; Mochalin, V.; Gogotsi, Y. Dispersions of Two-Dimensional Titanium Carbide MXene in Organic Solvents. *Chem. Mater.* **2017**, *29* (4), 1632−1640.

(23) Zhang, Q.; Lai, H.; Fan, R.; Ji, P.; Li, H. High Concentration of $Ti_3C_2T_x$ MXene in Organic Solvent. *ACS Nano* **2021**, *15* (3), 5249−5262.

(24) Zhang, C.; McKeon, L.; Kremer, M.; Park, S.; Ronan, O.; Seral-Ascaso, A.; Barwich, S.; Coileain, C.; McEvoy, N.; Nerl, H.; Anasori, B.; Coleman, J.; Gogotsi, Y.; Nicolosi, V. Additive-Free MXene Inks and Direct Printing of Micro-Supercapacitors. *Nat. Commun.* **2019**, *10* (1), 1795.

(25) Wu, N.; Li, X.; Liu, S.; Zhang, M.; Ouyang, S. Effect of Hydrogen Bonding on the Surface Tension Properties of Binary Mixture (Acetone-Water) by Raman Spectroscopy. *Appl. Sci.* **2019**, *9* (6), 1235.

(26) Sun, N.; Guan, Z.; Zhu, Q.; Anasori, B.; Gogotsi, Y.; Xu, B. Enhanced Ionic Accessibility of Flexible MXene Electrodes Produced by Natural Sedimentation. *Nano-Micro Lett.* **2020**, *12* (1). DOI: 10.1007/s40820-020-00426-0

(27) Shi, D.; Yang, M.; Zhang, B.; Ai, Z.; Hu, H.; Shao, Y.; Shen, J.; Wu, Y.; Hao, X. BCN-Assisted Built-In Electric Field in Hetero-structure: An Innovative Path for Broadening the Voltage Window of Aqueous Supercapacitor. *Adv. Funct. Mater.* **2021**, 2108843.

(28) Li, H.; Hou, Y.; Wang, F.; Lohe, M. R.; Zhuang, X.; Niu, L.; Feng, X. Flexible All-Solid-State Supercapacitors with High Volumetric Capacitances Boosted by Solution Processable MXene and Electrochemically Exfoliated Graphene. *Adv. Energy Mater.* **2017**, *7* (4), 1601847.

(29) Feng, X.; Ning, J.; Xia, M.; Guo, H.; Zhou, Y.; Wang, D.; Zhang, J.; Hao, Y. A High Operating Voltage Micro-Supercapacitor

Based on the Interlamellar Modulation Type Ti$_3$C$_2$T$_x$ MXene. *Nanotechnology* **2021**, *32* (3), No. 035402.

(30) Wu, C.; Unnikrishnan, B.; Chen, I. W. P.; Harroun, S. G.; Chang, H. T.; Huang, C. C. Excellent Oxidation Resistive MXene Aqueous Ink for Micro-Supercapacitor Application. *Energy Storage Mater.* **2020**, *25*, 563−571.

(31) Xia, Q.; Fu, J.; Yun, J.; Mane, R.; Kim, K. High Volumetric Energy Density Annealed-MXene-Nickel Oxide/MXene Asymmetric Supercapacitor. *RSC Adv.* **2017**, *7* (18), 11000.

(32) Wang, J.; Li, F.; Zhu, F.; Schmidt, O. Recent Progress in Micro-Supercapacitor Design, Integration, and Functionalization. *Small Methods* **2018**, 1800367.

(33) Liu, D.; Jia, Z.; Wang, D. Preparation of Hierarchically Porous Carbon Nanosheet Composites with Graphene Conductive Scaffolds for Supercapacitors: An Electrostatic-Assistant Fabrication Strategy. *Carbon* **2016**, *100*, 664−677.

(34) Xie, Y.; Zhang, H.; Huang, H.; Wang, Z.; Xu, Z.; Zhao, H.; Wang, Y.; Chen, N.; Yang, W. High-Voltage Asymmetric MXene-Based On-Chip Micro-Supercapacitors. *Nano Energy* **2020**, *74*, 104928.

(35) Li, Q.; Wang, Q.; Li, L.; Yang, L.; Wang, Y.; Wang, X.; Fang, H. Femtosecond Laser-Etched MXene Microsupercapacitors with Double-Side Configuration via Arbitrary On- and Through-Substrate Connections. *Adv. Energy Mater.* **2020**, *10* (24), 2000470.